EVOLUTION AND USE OF COMBINED MECHANICAL AND THERMAL CODES FOR CRYOGENIC TURBOPUMP BEARINGS

Joe C. Cody, David E. Marty, and James D. Moore
Aerospace & Commercial Systems Directorate
SRS Technologies
Huntsville, AL 35806

ABSTRACT

Shaft bearing system analysis codes have been developed, improved, and used to investigate Space Shuttle Main Engine (SSME) Liquid Oxygen (LOX) turbopump bearing problems, and to support the Marshall Space Flight Center (MSFC) Bearing and Seal Materials Test (BSMT) program. Thermal network modeling uses the "SINDA" thermal code, and the modeling of bearing quasi-dynamic characteristics uses the "SHABERTH" bearing/shaft code. These codes are solved concurrently for a bearing/shaft system using software developed for this purpose. Simulation of the SSME LOX turbopump turbine and pump end bearings and the MSFC BSMT operating in liquid nitrogen (LN_2) and LOX has been done. The thermal network models include the bearing components, bearing carriers, shaft, housing, frictional heat, and viscous fluid energy. A cage model has recently been included to account for heat generation between the cage and rolling elements. Since most bearing surfaces operate at temperatures well above the coolant saturation temperature, and move at high speed relative to the coolant, forced convection boiling is the dominant mechanism for heat removal. Improved modeling of forced convection film boiling has been incorporated to take into account the local vapor generation at the high temperature surfaces. Bearing preloads in the pump and tester are provided by preload springs. As bearing operating clearances and contact angles change due to thermal effects and loading, the bearing preload changes with these varying conditions. These characteristics have been modeled and are included in the overall system models. Results from these models indicate an operational limit which, if exceeded, predicts a thermal excursion. Beyond these limiting conditions the thermal and mechanical models fail to arrive at a compatible solution. Simply stated, for these conditions the heat generated in the bearing exceeds the cooling capability of the coolant system. Limiting conditions predicted for the BSMT in LN_2 have correlated well with experimental data. Predictions for BSMT operation in LOX will be compared with upcoming LOX tests.

INTRODUCTION

The development of system modeling capability for high speed bearings operating in cryogenics, supports the overall MSFC bearing and seal materials development program which is designed to formulate and experimentally verify failure mechanisms and life prediction models for high speed bearing shaft systems operating in cryogenics. The modeling effort supports the BSMT program, and the development and improvement of the SSME LOX turbopumps.

Modeling the operating characteristics of the SSME LOX pump and BSMT bearing shaft characteristics is a complex task requiring the application of multi-disciplined engineering capabilities. Combinations of deflection, dynamic, stress, thermal, and fluid analyses are involved in the determination of the bearing shaft system operating characteristics. Due to this complexity, modeling capabilities have improved in an evolutionary fashion as new experimental data are obtained and understanding of system operation matures.

As the bearing shaft system searches for thermal and mechanical equilibrium, internal clearances change due to thermal gradients, and external loads change. These and other changes such as contact angle, change the bearing operating preload. The mechanical code has been updated to account for preload changes due to these operational changes. Thermal models have been improved to account for two phase flow conditions and can be run with the inlet coolant saturated. The pressure loss across the bearings and the corresponding influence on saturation temperature and other fluid properties are considered. The method for estimating the local heat transfer coefficient has been improved to account for local vapor quality. The cage has been modeled to provide simulation of heat generation, due to cage and ball contact, and the resulting heating effects on component temperatures.

Models of the MSFC BSMT operating in LN_2 have successfully predicted thermal excursions that have correlated well with experiment. Predictions for the tester operating in LOX have also been made to support upcoming tests of this BSMT in LOX.

Model Descriptions

The internal configuration of the MSFC BSMT is shown in Figure 1. Since the bearing pairs are similar, only one pair is modeled. The coolant flow enters a manifold at each end of the tester, flows through each bearing pair and exits via a common flow path. Although the tester was originally designed for radial and axial loading, current and planned tests are limited to axial loads. Since this produces an axially symmetrical bearing load, a radial section of the system is thermally modeled.

The bearing shaft configuration of the SSME HPOTP is shown in Figure 2. As with the tester two pairs of angular contact ball bearings are used. The two pairs are different however, with 45 mm bore bearings at the pump end and 57 mm bearings at the turbine end. The "SHABERTH" (Reference 1) model of this system includes all four bearings and the shaft. The pump end bearings are cooled by flow from the preburner pump that passes through a damping seal before entering the bearings. The turbine end bearings are cooled by flow passing through the hollow shaft and distributed via a diverter plate to the entrance to bearing No. 4.

Although the thermal networks for all bearings are similar, differences occur in the support structure for the tester, pump end and turbine end bearings. In addition both LOX and LN_2 coolants are included in the tester models. A typical nodal representation of the inner race, ball, cage and outer race for the 57 mm HPOTP turbine end bearing is shown in Figure 3. There are 546 nodes in the model. Surface nodes are connected by appropriate thermal resistors to the cryogenic fluid. Heat transfer coefficients are selected to represent the appropriate fluid heat transfer regime based on the node surface temperatures and the fluid saturation temperature. The cage is represented by nine nodes and is thermally connected to the ball and coolant flow. At this stage of development the cage is not thermally connected to the outer race. The fluid drag force acting on the cage is estimated and assumed to be equally shared by each ball. This force is used with the cage to ball friction and relative velocity between cage and ball to estimate the heat generation at the cage to ball interface.

Considerable heat is generated in the flow circuit due to working the fluid. The balls translate and spin through the fluid, the cage pockets cause considerable fluid drag, the inner race spins relative to the fluid, and the fluid rotates relative to the outer race. The relative rotational speed of the fluid and ball train is an important consideration in estimating cage drag and fluid work. Each bearing system is different in this respect. The HPOTP pump end bearing coolant flow passes through a rotating seal that imparts rotation to the coolant upstream of the first bearing. The turbine end coolant flow passes through a diverter plate rotating at shaft speed. The plate is designed to match the tangential component of fluid velocity with the tangential velocity of the ball train. The tester coolant flow is introduced radially and flows inward before passing through a bearing pair. The rotating shaft and slinger impart a rotation to the flow before it enters the bearings. In each case the tangential and axial velocities of the upstream flow are estimated for calculation of fluid heat generation. Heat generated due to fluid work in the downstream bearings is estimated in a similar manner. The other source of heat generated in the bearings is the heat generated at the rolling element contacts. These values are obtained from the "SHABERTH" bearing code.

Surface to Fluid Heat Transfer

The following procedure outlines the method currently used to estimate the heat transfer coefficients in the bearing thermal models. Locally at the heat transfer surface the fluid can be liquid, vapor or a combination depending on the surface temperature and fluid saturation temperature. The surface heat rate to the adjacent fluid for any surface element is:

1) $q = hA_e (t_w - t_s)$

t_w, t_s = Surface and saturation temperature
h = Heat transfer coefficient
A_e = Surface area of the element.

If (t_w + 2.78°C or (5°F)) < t_s liquid is assumed to exist at the surface and forced convection heat transfer coefficients based on liquid properties are used. If this condition is not satisfied then some quantity of vapor exists at the interface. The quantity of vapor is estimated:

2) $$\dot{m}_v = \frac{hA(t_w - t_s)}{h_{fg} + (t_s - t_b)\, Cp}$$

h_{fg} = The latent heat of vaporization at the local pressure and saturation temperature
t_b = The fluid bulk temperature
Cp = The specific heat of the liquid
A = Surface area representative of the flow passage.

The experimental results of Hendrix et al are correlated (Reference 2) as:

3) $$\frac{Nu_{exp}}{Nu_{cal}} = \exp[.185 - .215\ \ell n\ x - .00767\ (\ell n\ x)^2]$$

x = Vapor quality.

Nu_{exp} is the experimentally derived Nusselt number and the calculated Nusselt number for the correlation is:

4) $$Nu_{cal} = .026\ N_{Re_{v,s,p}}^{0.8}\ N_{Pr_v}^{0.33}\ \left(\frac{\mu_v}{\mu_w}\right)^{0.14}$$

$N_{Re_{v,s,p}}$ = Single phase Reynolds Number with vapor properties evaluated at saturation conditions

N_{Pr_v} = Prandtl number with vapor properties at saturation conditions

μ_v, μ_w = Vapor viscosity evaluated at saturation and element surface temperatures

The vapor quality X is defined as:

$$5) \quad X = \frac{\dot{m}_v}{\dot{m}_f}$$

With known surface (tw) and saturation (ts) temperatures, Equations 2, 3, 4 and 5 can be solved for the ratio of experimental to calculated Nusselt numbers. Since the above correlation was developed for flow in tubes, and the bearing has considerably more complex flow geometry, the above ratio of experimental to calculated Nusselt numbers is used with correlations more representative of bearing geometry. For the ball, Katsnellson's equation for spheres is used and for surfaces other than the rolling element the Dittus Boelter equation with vapor properties evaluated at the film temperature is used to provide a more conservative estimate of the heat transfer coefficient. Although not rigorous, this method provides an estimate of two phase heat transfer coefficients including local quality, which is dependent on coolant mass flow and subcooling, and provides model results consistent with the BSMT performance data.

Mechanical/Thermal Model Iterative Technique

The SHABERTH mechanical code and the SINDA (Reference 3) thermal code have been coupled to determine a mechanical/ thermal solution for a bearing pair. Bearing temperature and load are interrelated , the temperature affects the differential thermal growth of the bearing components which increases the internal loads. Higher internal loads causes increased frictional heat. This increased heat causes higher component temperatures from the thermal code. Thus, the output from the mechanical model updates the thermal model and the output from the thermal model is used to update the mechanical model. An executive control program was written to perform this iteration using FORTRAN code and Job Control Language (JCL), compatible with MSFC's IBM/CRAY computer system.

The interaction of the mechanical and thermal models is illustrated for the turbine end bearings in Figure 4. The user is to supply an initial estimate of the bearing component temperatures for the SHABERTH model. The program then calculates the bearing operating conditions for those temperatures. The frictional heat is then used to update the thermal model. The Bearing #3 thermal model calculates new temperatures which updates the Bearing #3 temperatures in the mechanical model. With these temperatures new operating conditions for

the bearing pair are determined and the frictional heat is used to update the thermal model for Bearing #4. The thermal model then predicts new temperatures for Bearing #4. The executive control program then compares the new and old temperatures for both bearings. If the new and old temperatures for Bearing #3 and those for Bearing #4 respectively compare withing 2°C (3.6°F) a converged solution is found. If any set of bearing temperatures do not agree within 2°C (3.6°F), the program checks to see if any temperature has exceeded 1000°C (1832°F). If this condition is exceeded the program stops and no compatible solution exists. If all the temperatures are less than 1000°C (1832°F) the executive control program checks the loop counter; if it is greater than 11 the program stops. The user then evaluates the temperatures to determine if they are converging or diverging. If further iterations are desired the user can manually update the mechanical model with the latest temperatures and start the executive control program again. If the loop counter is less than 11 the control program updates the mechanical model automatically and continues execution. Figure 5 illustrates graphically the iteration between the mechanical and thermal model for a converged solution. Figure 6 illustrates the iteration process for a diverged solution where the temperature of the ball will exceed 1000°C (1832°F).

Modeling of Operating Preload Characteristics

The bearing mechanical code has been modified to consider effects of preloading springs in duplex bearing pairs. Bearing preloading in duplex ball bearing sets is accomplished by generating an internal axial load. The load is generated by forceably offsetting the inner and outer races to compress the rolling elements. Some amount of preloading is desirable because bearing stiffness is increased and ball skidding effects are minimized. However, loss of bearing operating clearance, from thermal and dynamic effects, can generate internal loads in excess of design preloads. To maintain bearing preload, while compensating for these varying effects, the LOX pump bearings utilize floating outer races axially loaded by beam springs. Figure 7 shows the spring arrangement in the 45 mm pump end bearing set. The beam spring maintains an axial preload on the bearings while allowing the outer races to move to the point where the internal preload is balanced by the spring force. To properly model this configuration, the model input governing the axial offset of the inner and outer races, must be updated to reflect the amount of race offset corresponding to the current spring deflection. However, to avoid this time consuming manual iteration procedure, the SHABERTH software has been modified to internally account for bearing geometry changes due to temperature and other effects and the results this has on operating preload.

The preload spring model utilizes a root finding algorithm that iteratively modifies the input data to reflect outer race axial travel. During each iteration, the bearing reaction force is compared to the calculated spring force. The spring force is determined by multiplying

the spring constant by the change in bearing deflection corresponding to the reaction force. The solution continues until a force balance is achieved. Figure 8 shows the thermal compensation effect of the preload spring in the 45 mm pump end bearing. These curves were generated by executing SHABERTH both with and without the "spring option" activated. The ball temperature was varied to simulate loss of internal clearance. The temperature of all other bearing components was -173°C (-280°F). Therefore, the ball temperatures and loads illustrated do not correspond to actual operating conditions. In a typical analysis, the model accounts for clearance changes from many sources including inner and outer race temperature changes. The figure illustrates that the preload spring reduces the rate of internal axial load increase with loss of bearing clearance. The 45 mm pump end bearings bottom the spring with approximately 5650 N (1270 lbs) axial load. When the spring bottoms no further thermal compensation is available and the rate of loading rapidly increases with further loss of internal clearance.

Comparison of Model Results and Test Data for MSFC's Bearing and Seal Materials Tester

The BSMT bearing/shaft model was used to estimate bearing operating limits and to guide the establishment of redline temperatures for tester operation in LN_2 and LOX. The LN_2 tests have been completed, and comparisons of model results and tester data are presented, in addition model predictions for planned LOX tests are provided. The conditions for which thermal excursions will occur were of special interest for both LN_2 and LOX tests. Figures 9 and 10 are comparisons of model and test data for the LN_2 tests. Included are model results for the BSMT operating in LOX. The difference in outer race and inlet coolant temperatures is plotted versus the difference in saturated and inlet enthalpy. The tester configuration for the LN_2 and upcoming LOX tests are the same with the exception of the bearings. The LN_2 tests were conducted with Phase I turbopump turbine end bearings, and the LOX tests will use Phase II turbine end bearings. The bearing configurations are similar, both being 57 mm angular contact ball bearings. All dimensions are similar with the exception of increased clearance and inner race curvatures for the Phase II bearings. The model predicted a thermal excursion at approximately 23.3 KJ/Kg (10 BTU/lb) of subcooled enthalpy in LN_2. As shown in Figure 9 the number 2 bearing experienced a thermal excursion at approximately 16.3 kJ/kg (7 BTU/lb) (Test 2451). In subsequent tests, the bearing 2 redline was removed. Bearing 3 experienced a thermal excursion at approximately 27.9 kJ/kg (12 BTU/lb) as shown in Figure 10 (Test 2471). After this test, temperature redlines were also removed from bearing 3, allowing higher temperature operation without test cutoff. Further thermal excursions were not experienced even though subcooling was reduced to zero. Revising the model to reflect 0.102 mm (4 mils) of diametrical ball wear allowed a thermally stable operating condition at higher component temperatures for zero subcooling. This is in agreement with the observed tester operation. The dashed line in

Figures 9 and 10 indicates possible outer race temperatures as the bearing wears to provide additional operating clearance. This indicates a thermal excursion can occur with a "new" bearing, recover and continue to operate at higher temperature as internal wear increases the clearance. This, however, must be verified by additional tests.

Modeling results with LOX as the coolant are also provided for comparison. For the conditions investigated, the Phase II design operating in LOX has a lower outer race temperature rise over the inlet coolant temperature and can operate at less subcooling before a thermal excursion occurs than can the Phase I design operating in LN_2. The increased clearance in the Phase II bearings accounts in part for the improved performance. In addition the effects of pressure on the thermal stability of the bearing must be considered. Since inlet subcooling is controlled by tester pressure, low inlet subcooling requires reductions in inlet pressure for a given value of inlet coolant temperature. Consequently, the lower the inlet temperature, the lower the pressure for a specific value of subcooling. Due to the pressure effect on heat transfer, lower inlet temperatures require larger values of subcooling to maintain thermal stability.

Model Results for High Pressure Oxidizer Turbopump Bearings

The mechanical/thermal model was used to evaluate operating conditions for both the turbine end and pump end bearings of the SSME HPOTP. The turbine end bearing model was used to evaluate the effects of contact friction between the races and ball on operating characteristics. The effect of flow rate was investigated using the pump end bearings. The mechanical/thermal model was operated with the "spring option" which considers the preload springs adjusting to operating conditions.

The HPOTP turbine end bearings were investigated for the conditions shown in Table 1. The model was operated using dry friction which was increased to determine a stable operating limit condition. Shown in Table 1 are the average component temperatures, maximum average track temperatures, total axial and radial loads on the bearings, and the total inner and outer race heat generation for each bearing for the coefficient of friction shown. The model predicted that bearing #3 will carry about 75% of the radial load due to shaft deflection and increased radial stiffness caused by loss of clearance due to thermal growth. The model also predicted that the bearing pair would experience a thermal excursion before the preload springs bottomed. The axial force needed to fully compress the Phase II turbine end springs is $\sim$8900 N ($\sim$2000 lbs). The maximum axial load determined for a thermally stable solution was $\sim$6850 N ($\sim$1540 lbs). For these conditions, the maximum Hertz Stress was $\sim$3310 N/mm^2 ($\sim$480 Kpsi) for bearing #3 and $\sim$2720 N/mm^2 ($\sim$395 Kpsi) for bearing #4.

To illustrate the effect of coolant flow on bearing operation, the pump end bearings were investigated using a coefficient of friction of 0.460, saturated inlet coolant at 2.3 N/mm^2 (334 psia) and saturated exit at 1.9 N/mm^2 (276 psia). The initial chilled preload was 2135 N (480 lb). Shown in Figure 11 are the average component temperatures as a function of coolant flow. The range of flow was chosen to be representative of the flow rates in the HPOTP pump end bearings. For these conditions the lowest flow rate that would maintain a stable solution was 1.81 Kg/s (4 lb/s). At this flow, bearing #2 had thermally stiffened such that it supported virtually all of the radial load. The preload spring was compressed to about 5000 N (1124 lb). The force needed to fully compress (bottom) the Phase II pump end spring is ∿5650 N (1270 lb). Thus, the Phase II pump end bearings will experience a thermal excursion before the preload spring bottoms. The maximum contact stress predicted for this case is for the bearing #2 inner race of 3240 N/mm^2 (470 Kpsi). Figure 11 shows that the component operating temperatures can be significantly lowered by increasing the coolant flow rate. When the temperatures are decreased the internal loads on the bearing are less, for example, at 5.4 kg/s (12 lb/s) the axial force on the preload spring is 3930 N (884 lb). Thus, by increasing the flow rate from 1.81 kg/s (4 lb/s) to 5.4 kg/s (12 lb/s) the axial force on the pump end bearings can be decreased by ∿21%.

CONCLUSIONS

Improvements in the capability for modeling high speed bearing shaft systems operating in cryogenics have been developed. Without the insight provided by the BSMT and other tests in LOX these improvements would not be available. By modeling the local effects of vapor quality on the two phase heat transfer coefficients and the thermal and load effects on bearing preload, bearing temperatures, thermal excursions, and other operating characteristics can be more realistically predicted.

These bearing codes provide valuable tools for assessing the design characteristics of bearing shaft systems operating in cryogenics including the evaluation of new bearing material candidates. Although comprehensive in the combined treatment of thermal and mechanical characteristics, additional improvements are needed. The time dependent characteristics of the cage need to be modeled to improve the estimate of heat generation due to cage/ball and cage/race contact and also to improve the estimates for cage loading. Improved analyses for estimating the fluid drag on the cage and other bearing components are needed. Heat generation due to ball skid caused by unloaded balls entering a load zone needs additional work. Additional data from the MSFC BSMT in LOX is required for further model verification.

References

1. SHABERTH Computer Program Operation Manual, Technical Report AFAPL-TR-76-90, October 1976.

2. Brentari, E. G.; Giarratano, P. J.; and Smith, R. V.: Boiling Heat Transfer for Oxygen, Nitrogen, Hydrogen, and Helium. NBS Technical Note 317., Sept. 1965.

3. SINDA Engineering Program Manual (Contract No. NAS9-10435), June 1971.

TABLE 1 HPOTP TURBINE END BEARINGS (57 mm PHASE II) OPERATING CONDITIONS

	COEFFICIENT OF FRICTION							
	0.200		0.250		0.300		0.335	
	BRG 3	BRG 4	BRG 3	BRG 4	BRG 3	BRG 4	BRG 3	BRG 4
AVG BALL AVG I.R. AVG O.R.	52 °C (126 °F) -69 °C (-92 °F) -118 °C (-181 °F)	-50 °C (-59 °F) -104 °C (-156 °F) -109 °C (-221°F)	100 °C (212 °F) -48 °C (-54 °F) -109 °C (-164 °F)	-19 °C (-3 °F) -88 °C (-126 °) -136 °C (-213 °F)	129 °C (265 °F) -22 °C (-8°F) -103 °C (-154 °F)	31 °C (88 °F) -63 °C (-82 °F) -130 °C (-203 °F)	157 °C (315 °F) -9 °C (15 °F) -97 °C (-142 °F)	77 °C (170 °F) -42 °C (-44 °F) -122 °C (-188 °F)
MAX BALL MAX I.R. MAX O.R.	193 °C (380 °F) 128 °C (262 °F) 17 °C (62 °F)	40 °C (104 °F) 37 °C (99 °F) -89 °C (-129 °F)	248 °C (479 °F) 174 °C (345 °F) 50 °C (122 °F)	95 °C (203 °F) 102 °C (216 °F) -69 °C (-93 °F)	299 °C (570 °F) 263 °C (506 °F) 59 °C (139 °F)	174 °C (345 °F) 189 °C (372 °F) -37 °C (-35 °F)	358 °C (676 °F) 329 °C (624 °F) 71 °C (160 °F)	239 °C (462 °F) 258 °C (497 °F) -4 °C (25 °F)
AXIAL LOAD	5996 N (1348 LB)	5947 N (1337 LB)	6174 N (1388 LB)	6120 N (1376 LB)	6619 N (1488 LB)	6574 N (1478 LB)	6881 N (1547 LB)	6836 N (1537 LB)
RADIAL LOAD	10190 N (2291 LB)	4137 N (930 LB)	10448 N (2349 LB)	3919 N (881 LB)	10960 N (2464 LB)	3487 N (784 LB)	11240 N (2527 LB)	3242 N (729 LB)
TOTAL I.R. HEAT GENERATION	4304 WATTS (4.08 BTU/SEC)	2965 WATTS (2.81 BTU/SEC)	5127 WATTS (4.86 BTU/SEC)	3777 WATTS (3.58 BTU/SEC)	5665 WATTS (5.37 BTU/SEC)	4832 WATTS (4.58 BTU/SEC)	6056 WATTS (5.74 BTU/SEC)	5613 WATTS (5.32 BTU/SEC)
TOTAL O.R. HEAT GENERATION	3724 WATTS (3.53 BTU/SEC)	1466 WATTS (1.39 BTU/SEC)	4347 WATTS (4.12 BTU/SEC)	1910 WATTS (1.81 BTU/SEC)	4758 WATTS (4.51 BTU/SEC)	2616 WATTS (2.48 BTU/SEC)	5064 WATTS (4.80 BTU/SEC)	3207 WATTS (3.04 BTU/SEC)
MAXIMUM HERTZ STRESS INNER RACE OUTER RACE	3246 N/mm^2 (470740 PSI) 2706 N/mm^2 (392440 PSI)	2717 N/mm^2 (394130 PSI) 2341 N/mm^2 (339470 PSI)	3248 N/mm^2 (470580 PSI) 2704 N/mm^2 (392180 PSI)	2708 N/mm^2 (392760 PSI) 2333 N/mm^2 (338420 PSI)	3284 N/mm^2 (476320 PSI) 2733 N/mm^2 (396410 PSI)	2718 N/mm^2 (394220 PSI) 2339 N/mm^2 (339300 PSI)	3310 N/mm^2 (480010 PSI) 2751 N/mm^2 (398920 PSI)	2724 N/mm^2 (395020 PSI) 2342 N/mm^2 (339710 PSI)
BEARING #3 COOLANT EXIT TEMPERATURE	-144.4 °C (-228.0 °F)		-143.9 °C (-227.0 °F)		-143.4 °C (-226.1 °F)		-142.9 °C (-225.2 °F)	

2.1 KG/SEC (4.6 LB/SEC) COOLANT FLOW RATE
BEARING #4 COOLANT INLET = -151 °C (-240 °F) AT 2.4 N/mm^2 (350 PSIA)
BEARING #3 COOLANT EXIT AT 2.1 N/mm^2 (304 PSIA)
OPERATED WITH DRY FRICTION
4670 N (1050 LB.) INITIAL CHILLED PRELOAD

FIGURE 1 MSFC BEARING AND SEAL MATERIALS TESTER CONFIGURATION

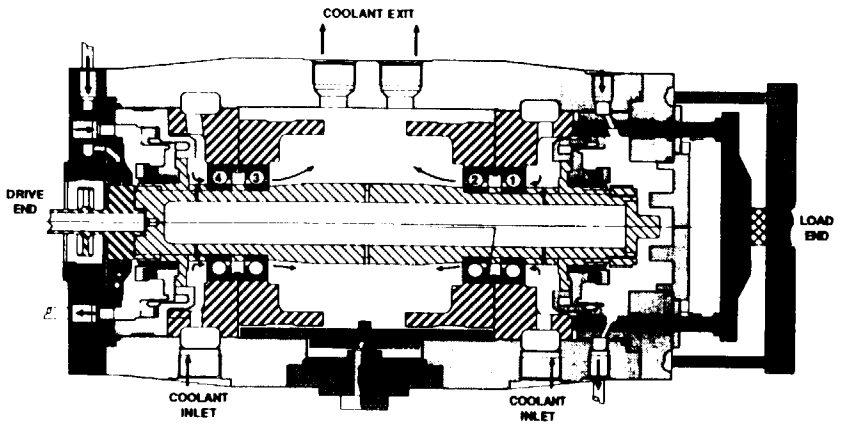

FIGURE 2 SSME LOX TURBOPUMP BEARING/SHAFT CONFIGURATION

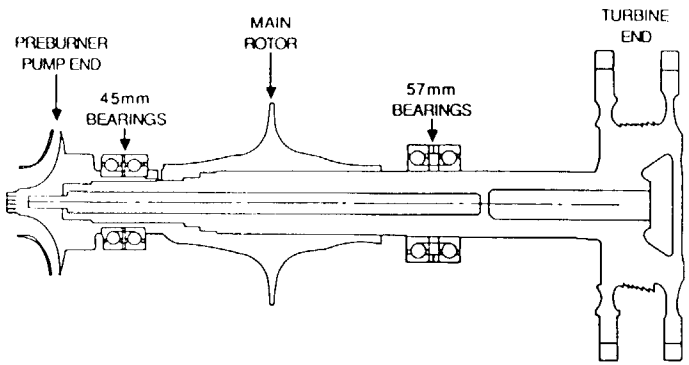

FIGURE 3 TURBINE END 57mm BEARING THERMAL NODES

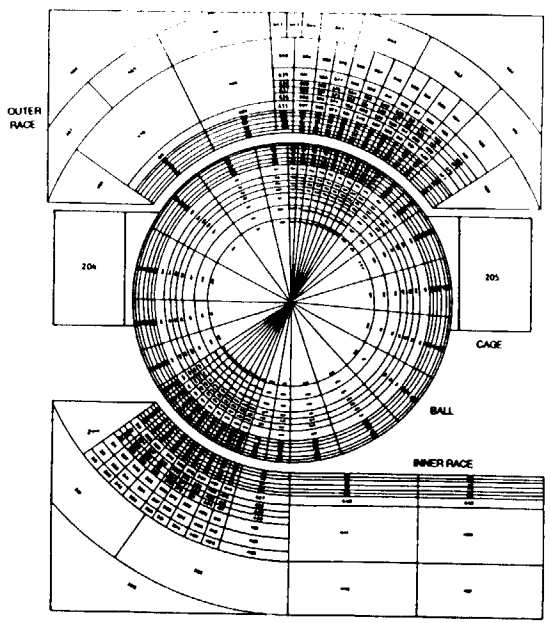

FIGURE 4 FLOWCHART OF THE MECHANICAL/THERMAL MODEL CONTROL PROGRAM

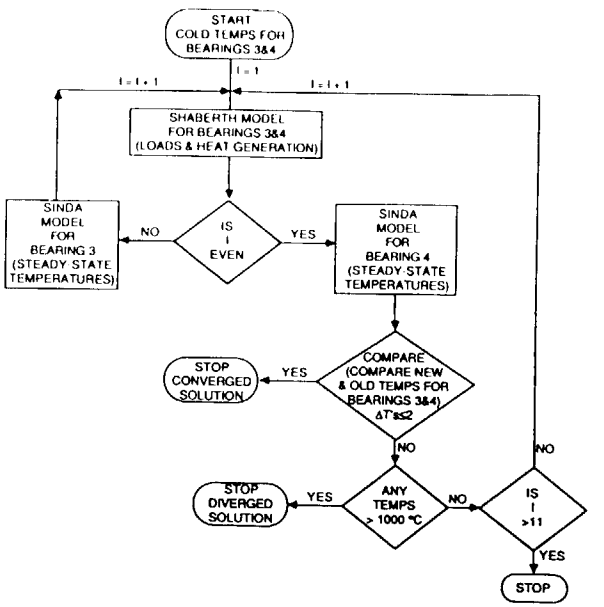

FIGURE 5 ITERATION PROCESS BETWEEN SHABERTH AND SINDA FOR A CONVERGED SOLUTION

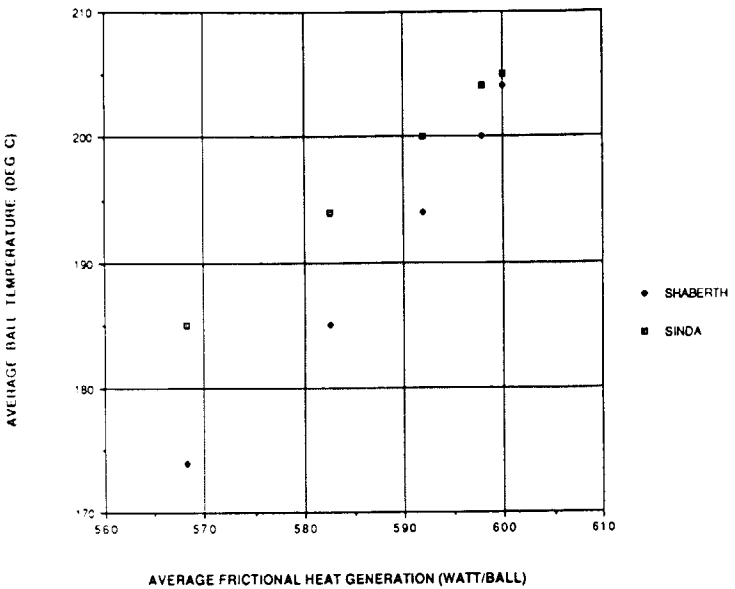

FIGURE 6 ITERATION PROCESS BETWEEN SHABERTH AND SINDA FOR A DIVERGING SOLUTION

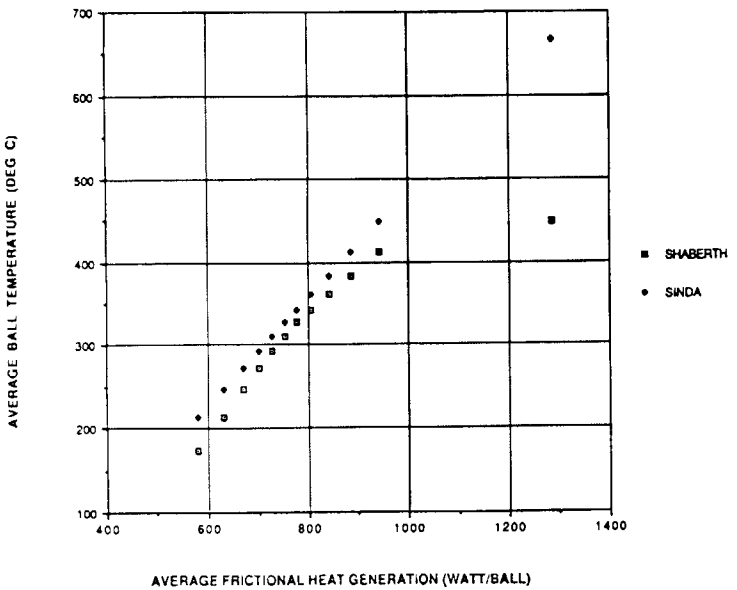

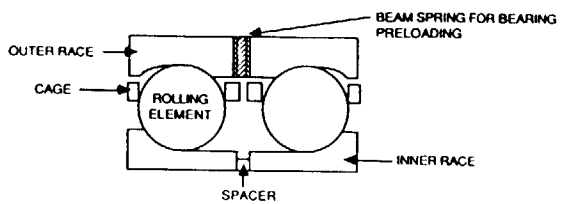

FIGURE 7 PRELOAD SPRING ARRANGEMENT IN THE 45 mm PUMP END BEARING SET

FIGURE 8 ILL[illegible] PRING MODEL FOR 45[illegible] BEAR[illegible] SET

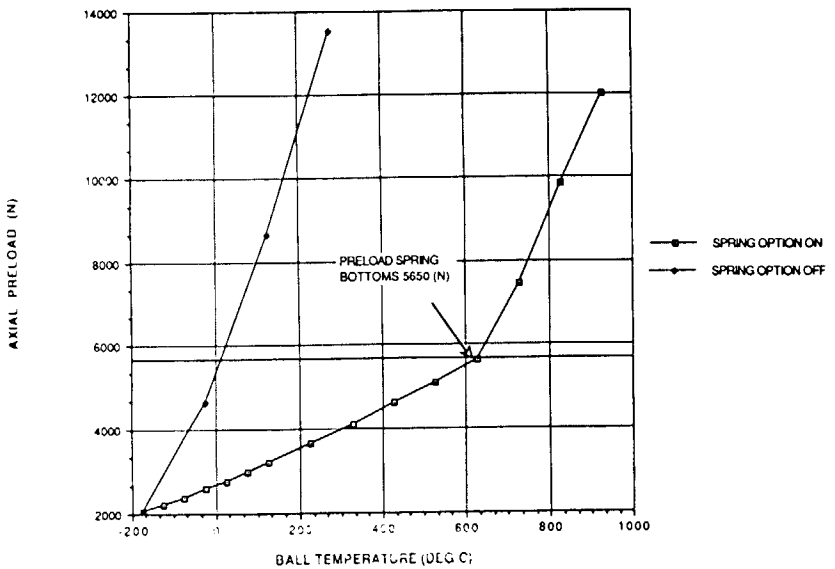

FIGURE 9

EFFECT OF INLET COOLANT CAPACITY ON BEARING #2 OUTER RACE/COOLANT DELTA T

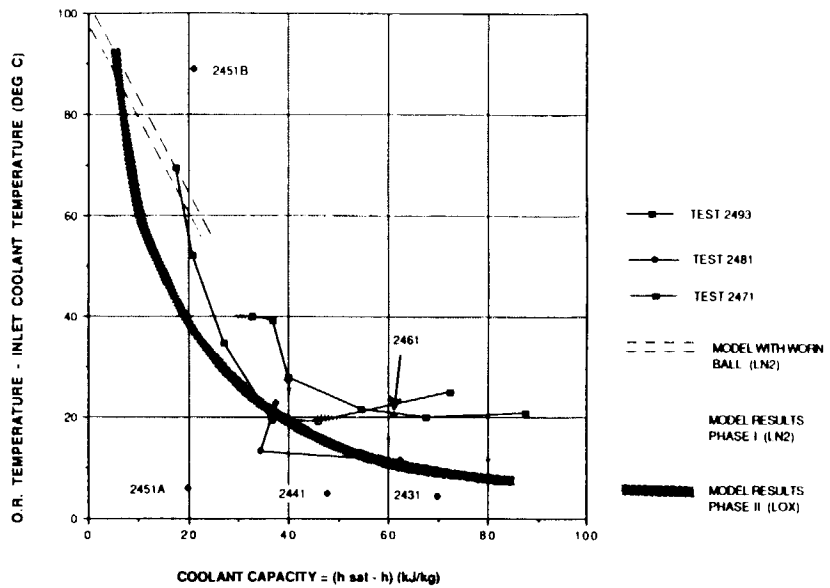

FIGURE 10

EFFECT OF INLET COOLANT CAPACITY ON BEARING #3 OUTER RACE/COOLANT DELTA T

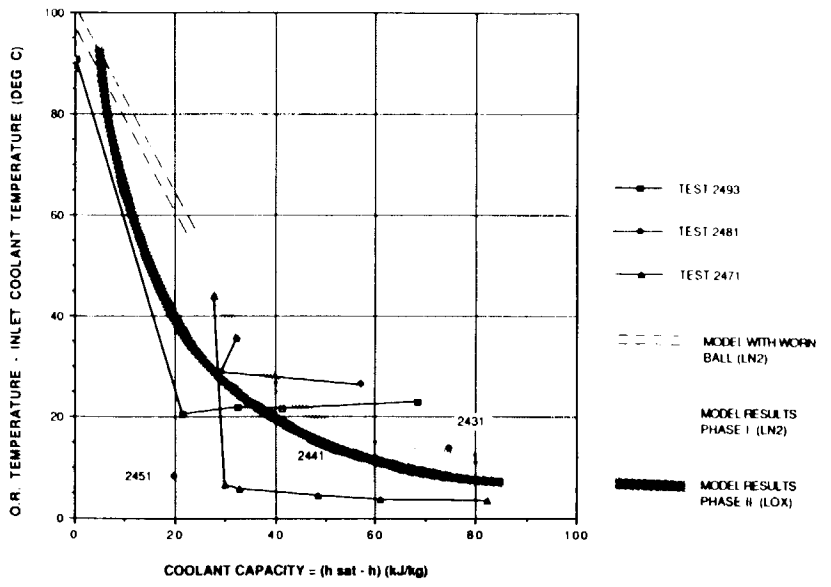

FIGURE 11 HPOTP BEARING #2 AVERAGE COMPONENT TEMPERATURES